



# Optimized multi-scale affine shape registration based on an unsupervised Bayesian classification

Khaoula Sakrani<sup>1</sup> · Sinda Elghoul<sup>1</sup> · Faouzi Ghorbel<sup>1</sup>

Received: 2 August 2022 / Revised: 2 August 2022 / Accepted: 6 February 2023 /  
Published online: 5 June 2023

© The Author(s), under exclusive licence to Springer Science+Business Media, LLC, part of Springer Nature 2023

## Abstract

Here, we intend to introduce an efficient, robust curve alignment algorithm with respect to the group of special affine transformations of the plane denoted by  $SA(2,R)$ . Such a group of transformations is known to be well model the pose of 3D scene when objects are far from the visual sensor relatively to their sizes. Its numerical robustness lies in its multi-scale approach and its precision comes from the automatic and unsupervised Bayesian selection of the efficient scales in the sense of  $L_2$  metric. In this work, We prove its high alignment performance on the most studied image databases such as MPEG-7, MCD, Kimia-99, Kimia216, ETH-80, and the Swedish leaf experimentally. The unsupervised Bayesian classification is based on the well-known multiclass Expectation-Maximization algorithm.

**Keywords** Affine transformations · A normalised affine arc-length parametrization · ACM Algorithm · Multi-scale registrations · Multiclass Expectation Maximisation (Multiclass-EM) · Unsupervised bayesian classification

## 1 Introduction

The shape registration process is a fundamental computer vision task with broad applications in many fields, including robot navigation [82], medical image matching [31], face recognition [22, 81], Remote Sensing [85], large-scale 3D reconstruction and object tracking [41, 95]. Image registration is the alignment process of two or more images of the same object captured at different times, from different perspectives, or by different imaging machines. As input for the alignment, a reference image (fixed image) and another one named the target used for the transformation estimation. Mathematically, the shape registration is to determine the optimal spatial geometric transformations that yield the best alignment between these two inputs.

---

Sinda Elghoul and Faouzi Ghorbel contributed equally to this work.

✉ Khaoula Sakrani  
sakrani.khaoula@gmail.com

<sup>1</sup> CRISTAL Laboratory, GRIFT Research Group National School of Computer Science (ENSI), Manouba University, Manouba, 2010, Tunisia

Several registration algorithms were operated to determine the Euclidean transformation, also known as  $E(2)$ , presented by a rotation followed by a translation. However, to reconstruct a three-dimensional object from two of its projections, the transformation assembling them is frequently modeled by a planar homography [20]. Unfortunately, planar Equi-projective re-parametrization curves are required for the matching of curves up to a planar homography, which necessitates at least five numerical derivations [80]. This causes approximation errors equal to the value order of the quantities to estimate. For which, replacing the homography with the associated affine transformation is frequently proposed.

Consequently, if the object is planar and sufficiently distant from the camera, the pose can be approximated by a 2D special affine transformation  $SA(2,R)$  [11]. In this context, the ACMA (Affine Curve Matching Algorithm) is developed to estimate the special affine transformation to align 2D shapes [19]. To improve the robustness of this method's numerical approximations, we involve adding the multi-scale notion to the ACM Algorithm. However, we notice that most of the works have chosen the scale number empirically, which can cause information loss at a certain level of smoothing. Furthermore, in [64], we suggest applying the Binary Expectation Maximisation (Binary-EM) [14], which is a statistical method to adjust this choice. However, despite the improvement obtained through this adjustment process, the choice of the number of scales is still vast, and the execution time can still be improved.

This work aims to present a new Affine Multi-Scale Curve Registration (AMSCR) based on an unsupervised Bayesian classification. This method has two input curves (source image, target image) normalized sequentially with affine arc-length parametrization and smoothed. Then, we use the K-means and Elbow method to automate choosing the optimal class number. After that, we apply Multiclass-EM as a robust probability density estimator to find the best scales. Finally, the alignment process is still done by the ACM Algorithm. The AMSCR based on an unsupervised Bayesian classification enhances the registration process's complexity and performance.

The rest of the paper is structured as follows: Section 2 introduces the related work to our approach. Then, we recall the affine curve matching algorithm representing the affine arc length reparametrization and the pseudo-inverse matrix calculation in Section 3. Section 4 presents the Optimized Affine Multi-Scale Curve Registration (AMSCR) based on unsupervised Bayesian classification. In Section 6, we evaluate the accuracy of the proposed approaches in the task of shape retrieval using MPEG-7, MCD, Kimia-99, Kimia216, ETH-80, and the Swedish leaf database. Finally, the conclusion is presented in the end section.

## 2 Related work

Before delving into the specific details of our approach to shape registration, we will take a quick look at what's already out there. Shape matching is a topic that has received considerable attention in the scientific community. Indeed, there are numerous approaches related to Euclidean transformations. For example, in [27], the researchers suggest a new technique for rigid motion estimation based on Nyquist–Shannon theorem and B-spline approximation. In [35], they use the alignment criterion, Mutual Information (MI), to obtain the optimal transformation parameters, which defines a theoretical measure of the statistical dependencies between inputs. Another method for shape registration is named shape context invented by Belongie et al. [4]. The authors in [45] introduce an inner-distance shape context (IDSC) which is the shortest path between two feature points. In addition, Kang et al. [37] present

a global registration technique based on a graph for constructing a 2D mosaic from a collection of images. The graph represents temporal and spatial connectivity and demonstrates that the constructed graph can obtain the global registration by searching for an optimal path. [59] propose an approach based on Dynamic Programming (DP) for motion estimation where this method handles occluded, noisy, and distorted shapes. Additionally, in [66], the Analytical Fourier-Mellin Transform (AFMT) is adopted to define a complete family of invariant descriptors under any planar similarity. The researchers in [33] combine multiscale description and distance metrics in order to develop global descriptors MDM (multiscale distance matrix). This technique helps to obtain high efficiency and effectiveness in plant leaf retrieval. Shu et al. [69] suggested the multi-scale contour flexibility shape signature, which is a shape descriptor. It represents, however, the deformation characteristics of the 2D shape profile. Moreover, [60] introduce a non-rigid registration method in which motion estimation is cast into a feature matching problem using Graph Wavelets within the Log-Demons framework. In [91] present a new descriptor for non-rigid 2D shape matching based on Triangular Centroid Distances (TCDs). This method treats the occluded shape matching issue. Yang et al. [89] invent an approach named the invariant multi-scale descriptor for shape alignment. The DIR (distance interior ratio) is presented in [38] as a shape signature which is the intersection of line segments with the curve and a histogram alignment method. Yang and Yu [86] develop for shape identification a new method named multiscale Fourier descriptor based on triangular features. Benkhelifa et al. [5] introduce a new method called Generalized Curvature Scale Space (GCSS) to improve the almost complete property. In [1] Adamek et al. present a multi-scale convexity and concavity method for shape matching. A two-dimensional matrix represents the contour convexities and concavities at different scale levels. Wang and Gao [78] develop a method named Hierarchical String Cuts (HSCs) to satisfy the curve matching process. In [96] they build a descriptor named a weighted Fourier and wavelet-like descriptor based on inner distance shape context (IDSC-wFW) for shape matching. They followed these steps to implement the previously mentioned descriptor; the first step was rewriting the shape histograms of IDSC descriptors, changing the histogram of a point to the histogram of a field, and setting the field's histogram as a one-dimensional signal. Then transform this one-dimensional signal using a Fourier transform and a Haar wavelet. Finally, the results of the two transforms are linearly combined to form a new descriptor. Furthermore, in [97] the researchers present a new MultiScale Fourier Descriptor using Group Features (MSFDGF). Then, they use this descriptor and Shape Histograms to construct a global descriptor MSFDGF-SH. These prior approaches are only applicable to shapes up to a Euclidean or similarity transform. In practice, however, a camera captures the contour in an arbitrary orientation that certain geometric transformations may have distorted. As mentioned in [44], the affine transformation can simplify and approximate this distortion. Consequently, several methods for constructing representations of invariant objects under affine transformation have been developed. In [83] introduce a hybrid shape descriptor combining three invariants: area invariant, arc length invariant, and central distance invariant. Due to these three invariants, the description becomes representative and discriminative. Moreover, Cyganski et al. [12] propose a method for the affine transformation, where each contour is transformed to its affine invariant parametrization. Then, the over-determined system minimizes the Euclidean distance between two objects. Cyganski et al. [11] use the linear signal space decomposition technique for shape correspondence. In [3] they propose to use the oriented elliptical Gaussian neighborhoods to find the best correspondence between two curves from images. Pauwels et al. [58], Moons et al. [53] use the semi-differential invariant to develop affine invariant descriptions to estimate the

affine transformations. Gope et al. [29] introduce a method for affine shape matching using the area of mismatch, where this area is gated by aligning the curves optimally based on the minimum affine distance involving their specific points. The authors in [57] use The Hu invariant moment to describe a technique for affine global curves matching. Moreover, in [32] they use the Hungarian method and dynamic programming for points matching between two curves. Elghoul and Ghorbel [20] develop a fast approach for 2D special affine transformation based on a complete and stable descriptor. In [54] the researchers suggest an extended Scale-Invariant Feature Transform SIFT algorithm named Affine SIFT (ASIFT) for affine invariant matching. Kovalsky et al. [40] propose a technique for estimating the geometric and radiometric transformations for two objects. Bryner et al. [7] develop a novel framework for affine invariance based on Riemannian geometry. Afterward, they propose in [8] a Bayesian active contour with affine invariance. For the affine  $n$ -space curve, Liu [46] defines centro-affine invariant arc length and curvature functions. In [62] authors present the affine invariant pseudo-metric for surfaces.

There is also a large body of research work for iterative approaches proposed to improve the performance of point set registration. One of the most widely used point set matching algorithms is Iterative Closest Point (ICP) [6, 63]. In [61] the authors develop a multiview registration method for aligning a large data set. Also, in [48] the researchers propose an iterative method to estimate the transformation between two-point sets. First, they use a feature descriptor such as shape context to establish correspondence. Then the geometric transformation is done using a robust estimator  $L_{2E}$ . The Expectation-Maximization (EM) algorithm is an iterative, statistical, and probabilistic technique used to estimate the transformation between two-point sets. For this, Jian et al. [36] propose a framework for the rigid and non-rigid point sets registration problems. First, they describe the two input point sets using Gaussian mixture models. Then they align these two obtained Gaussian mixtures. In [56], Myronenko and Song suggest a probabilistic algorithm for rigid and non-rigid point sets registration named Coherent Point Drift (CPD). Moreover, [30] propose Multi-scale EM-ICP for an iterative point set mapping. Similarly, in [9] They use mixture models to represent the registration problem as maximum likelihood or Bayesian maximum a posteriori estimation problems. For this reason, they develop an EM-like technique to estimate transformations between the two mixture models. Chui et al. [10] model a feature-based registration algorithm called TPS–RPM (Thin-plate splines (TPS), Robust point matching (RPM)) to determine the correspondence between non-rigid point sets. Wang and Chen [77] propose fuzzy correspondences guided Gaussian mixture model for matching. In [47] the authors propose a novel technique that combines the shape context and Expectation-Maximization (EM) method to determine the geometric transformation parameters. Yang et al. [92] use a popular probability model, which is the Gaussian mixture model, to preserve the global structure of the point set. And they use the expectation-maximization algorithm to update model parameters. Lastly, Matuk et al. [51] build a Bayesian framework for shape alignment and transformation estimation.

### 3 Recall of affine curve matching algorithm

The affine curve matching algorithm (ACMA) [20] is a partial 2D affine curve alignment method based on a pseudo-inverse calculation. In the following part, we will recall the main steps of this technique. Starting with the shape normalization, which is done by the affine arc length re-parametrization [72] where enough points represent the input curves.

The number of result equations is higher than the unknown variables. Then, the computation of the pseudo-inversive matrix that allows the minimization of  $L_2$  distance and obtains an affine part-to-part registration curve.

### 3.1 Affine arc length re-parametrization

Generally, curves extracted from the different images of the same object are parameterized differently. Thus, to compare these two curves, they must have the same parametrization (same speed). It is obvious that a curve can be represented with several different parametrizations: For example, the ellipse can be represented by the two following parametrizations;

$$\begin{aligned}
 f_1(t) &= (x_1 = a \cos t; y_1 = b \sin t)_{t \in [0, 2\pi]} \\
 f_2(t) &= (x_2(u) = a \cos \log U; y_2(u) = b \sin \log U)_{U \in [1, e^{2\pi}]}
 \end{aligned}
 \tag{1}$$

with  $a, b$  positive real number, these two parametrizations describe the same ellipse curve ( $a$  and  $b$  are the minor axis and the major axis respectively). Therefore, we re-sample the contours with the normalized affine arc length function  $l(t)$  defined by [12]:

$$l(t) = \frac{1}{L} \int_0^t \|\det(\dot{f}(u), \ddot{f}(u))\|^{\frac{1}{3}} du
 \tag{2}$$

Let denote  $f(t)$  as the original parametrization of one of the two curves.  $L$  the affine totale length of the curve.  $\det$  represents the determinant operator.  $\dot{f}$  and  $\ddot{f}$  are respectively the first and second derivatives of  $f$ . Then, the relationship obtained between the two curves  $f$  and  $h$  after the normalization step is defined by:

$$h(l) = Af(l + l_0) + B
 \tag{3}$$

It is well known that simple planar curves can be classified into open and closed ones. In the first case, the starting point can be chosen from one of the two curve extremities. By fixing a given orientation in the plane,  $l_0$  defined in the formula (2) can be reduced to 0. For the second case, the curvature functions of each closed curve are estimated after maximization of the correlation between curvatures; it also becomes possible to make for  $l_0$  the zero value. Therefore, we will use the following relation:

$$h(l) = Af(l) + B
 \tag{4}$$

In Fig. 1, there are some examples of affine arc length re-parametrization with  $N = 100$ . The condition to find the best number of normalization points is studied in [21]. So we based the sampling choice on that work.

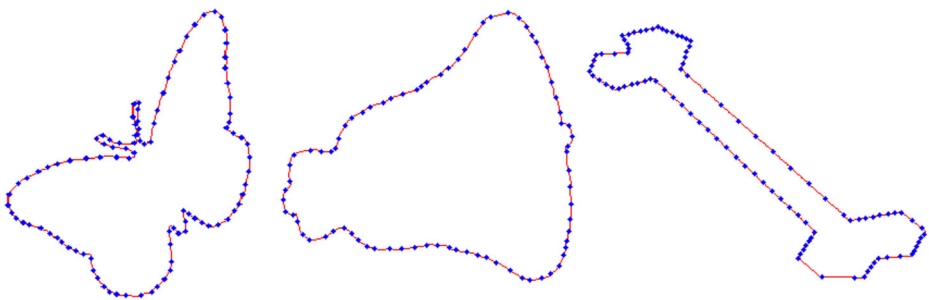


Fig. 1 Examples of affine arc length re-parametrization with  $N = 100$

### 3.2 Recall of pseudo-inverse Affine matrix calculation

To estimate the apparent movement between curves we calculate the pair  $A$  and  $B$  where  $A$  the special linear transformation and  $B$  the translation vector. The re-sampling of two curves by the normalized affine arc length provides  $2N$  equations and 6 unknown variables to the following rectangular system:

$$\begin{cases} h^x(l_1) = f^x(l_1)a_{11} + f^y(l_1)a_{12} + B^x \\ h^y(l_1) = f^x(l_1)a_{21} + f^y(l_1)a_{22} + B^y \\ \dots \\ h^x(l_N) = f^x(l_N)a_{11} + f^y(l_N)a_{12} + B^x \\ h^y(l_N) = f^x(l_N)a_{21} + f^y(l_N)a_{22} + B^y \end{cases} \tag{5}$$

with  $f^x(l_a)$ ,  $f^y(l_a)$  and  $h^x(l_a)$ ,  $h^y(l_a)$  ( $a=1..N$ ) are the two re-sampling cures related to the input shapes  $f(t)$  and  $h(t')$ ,  $A = (a_{ij})_{i,j=1,2}$  and  $B = (B^x, B^y)$ . We attempt to minimize the error between these two shapes, by calculating the pair  $A$  and  $B$  using:

$$\min_{(A,B)} = \|Af(l_a) + B - h(l_a)\|^2 \approx e \tag{6}$$

The system (3) can be written in matrix notation as follows:

$$H = DU \tag{7}$$

Where:  $H = [h_{l_1}^x h_{l_1}^y h_{l_2}^x h_{l_2}^y \dots h_{l_N}^x h_{l_N}^y]$ ;  $U = [a_{11} a_{12} a_{21} a_{22} B^x B^y]^t$  and

$$D = \begin{pmatrix} f^x(l_1) & f^y(l_1) & 0 & 0 & 1 & 0 \\ 0 & 0 & f^x(l_1) & f^y(l_1) & 0 & 1 \\ f^x(l_2) & f^y(l_2) & 0 & 0 & 1 & 0 \\ 0 & 0 & f^x(l_2) & f^y(l_2) & 0 & 1 \\ \vdots & \vdots & \vdots & \vdots & \vdots & \vdots \\ f^x(l_N) & f^y(l_N) & 0 & 0 & 1 & 0 \\ 0 & 0 & f^x(l_N) & f^y(l_N) & 0 & 1 \end{pmatrix} \tag{8}$$

This rectangular system can be solved by the pseudo-inverse calculation of the matrix  $D$ . The following formula determines the unknown vector  $U$ .

$$U = (D^t D)^{-1} D^t H \tag{9}$$

### 4 Optimized AMSCR based on unsupervised Bayesian classification

We noticed in [64] that we solved the problem of levels' choice by developing the adjusted AMSCR method using Binary-EM. In contrast, this method has a high computational cost, incredibly time-consuming. For this reason, we create an efficient unsupervised Bayesian approach to select the optimized smoothing levels by applying Multiclass-EM. For the choice of the Multiclass-EM class, we use the K-means and Elbow method to automate this choice (class number). This unsupervised 2D shape registration technique is developed according to the shape complexity. As a result, we obtain a shorter equation system that minimizes the errors. Figure 2 summarizes its workflow. Furthermore, this pipeline introduces how we choose the optimal scales using the Affine Multi-scale Curve Registration (AMSCR) based on unsupervised Bayesian classification. This method is divided into two parts; the first one presents the AMSCR process where it has as input pairs of source and

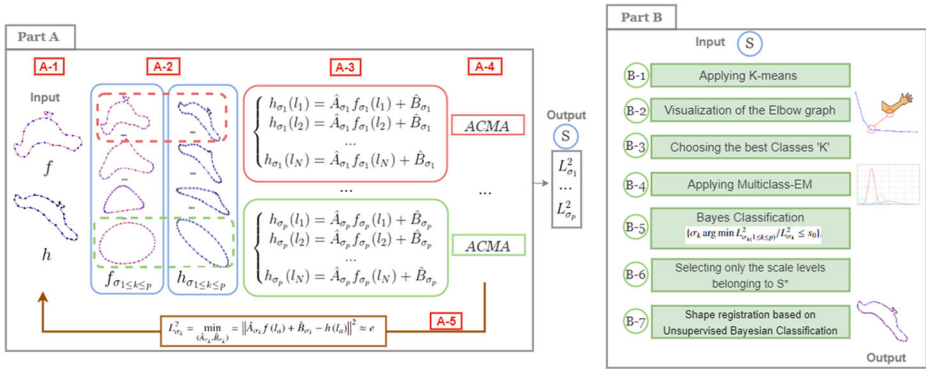


**Fig. 2** AMSCR based on unsupervised Bayesian classification

target 2D shapes, and the output is a vector  $S = \{\min L^2_{\sigma_i} (1 \leq i \leq p)\}$ . However, the second part presents the unsupervised Bayesian classification process.

**4.1 Part A: AMSCR process**

The affine Multi-Scale Curve Registration (AMSCR) procedure is summarized in the following steps.

- A-1: re-sampling each input shape  $f$  and  $h$  with affine arc-length parameterization.
- A-2: filter each component of the two re-sampling curves  $f^x_{\sigma_k}, f^y_{\sigma_k}$  and  $h^x_{\sigma_k}, h^y_{\sigma_k}$  with a Gaussian function  $g_{\sigma_k}$  at different levels of the scale ( $\sigma_k$ ) ( $1 \leq k \leq p$ ). Where  $p$  represents the number of smoothing levels. Hence, the resulting components related to the curve  $f_{\sigma_k}$  is represented by:

$$f^x_{\sigma}(l, \sigma) = f^x * g(l, \sigma) \quad f^y_{\sigma}(l, \sigma) = f^y * g(l, \sigma) \quad (10)$$

$$g(l, \sigma_k) = \frac{1}{2\pi\sigma_k^2} e^{-l^2/2\sigma_k^2} \quad (11)$$

With  $*$  denoting the convolution operation. The same process is adopted for the second curve  $h_{\sigma_k}$ .

- A-3: the retrieved  $p$  systems at each level ( $\sigma_k$ ) ( $1 \leq k \leq p$ ) formed by the following  $2N$  linear equations.

$$\begin{cases} h_{\sigma_1}(l_1) = \hat{A}_{\sigma_1} f_{\sigma_1}(l_1) + \hat{B}_{\sigma_1} \\ h_{\sigma_1}(l_2) = \hat{A}_{\sigma_1} f_{\sigma_1}(l_2) + \hat{B}_{\sigma_1} \\ \dots \\ h_{\sigma_1}(l_{N-1}) = \hat{A}_{\sigma_1} f_{\sigma_1}(l_{N-1}) + \hat{B}_{\sigma_1} \\ h_{\sigma_1}(l_N) = \hat{A}_{\sigma_1} f_{\sigma_1}(l_N) + \hat{B}_{\sigma_1} \end{cases} \quad \begin{cases} h_{\sigma_2}(l_1) = \hat{A}_{\sigma_2} f_{\sigma_2}(l_1) + \hat{B}_{\sigma_2} \\ h_{\sigma_2}(l_2) = \hat{A}_{\sigma_2} f_{\sigma_2}(l_2) + \hat{B}_{\sigma_2} \\ \dots \\ h_{\sigma_2}(l_{N-1}) = \hat{A}_{\sigma_2} f_{\sigma_2}(l_{N-1}) + \hat{B}_{\sigma_2} \\ h_{\sigma_2}(l_N) = \hat{A}_{\sigma_2} f_{\sigma_2}(l_N) + \hat{B}_{\sigma_2} \end{cases} \quad \dots \quad \begin{cases} h_{\sigma_p}(l_1) = \hat{A}_{\sigma_p} f_{\sigma_p}(l_1) + \hat{B}_{\sigma_p} \\ h_{\sigma_p}(l_2) = \hat{A}_{\sigma_p} f_{\sigma_p}(l_2) + \hat{B}_{\sigma_p} \\ \dots \\ h_{\sigma_p}(l_{N-1}) = \hat{A}_{\sigma_p} f_{\sigma_p}(l_{N-1}) + \hat{B}_{\sigma_p} \\ h_{\sigma_p}(l_N) = \hat{A}_{\sigma_p} f_{\sigma_p}(l_N) + \hat{B}_{\sigma_p} \end{cases} \quad (12)$$

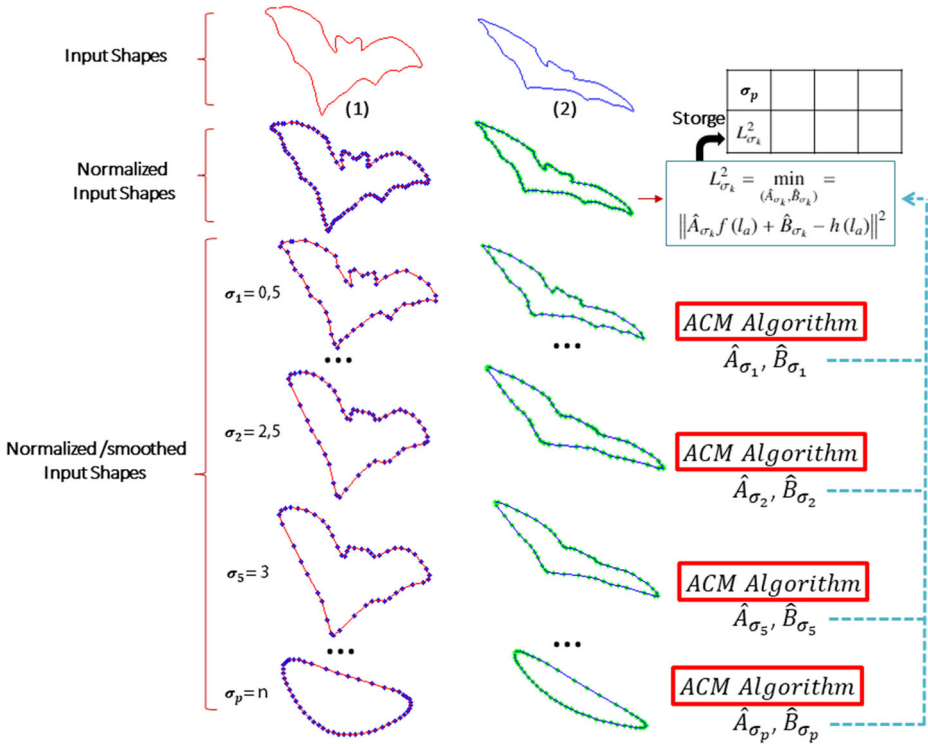


Fig. 3 Pipeline of Step 4,5

- A-4: by applying the ACM Algorithm [21] to each system indexed by  $k$ , we obtain the pair  $\hat{A}_{\sigma_k}$  and  $\hat{B}_{\sigma_k}$ , which are the elements of Special Affine group  $SA(2, R)$ .
- A-5: we use the pair  $\hat{A}_{\sigma_k}$  and  $\hat{B}_{\sigma_k}$  to compute the  $L_2$  distance (Euclidean distance) between the normalized input shape (source and target curves in step 1), then we obtain a vector where it storage all  $\sigma_k$  and the corresponding  $L^2_{\sigma_k}$ , which is denoted by:

$$L^2_{\sigma_k} = \min_{(\hat{A}_{\sigma_k}, \hat{B}_{\sigma_k})} \left\| \hat{A}_{\sigma_k} f(l_a) + \hat{B}_{\sigma_k} - h(l_a) \right\|^2 \approx e \tag{13}$$

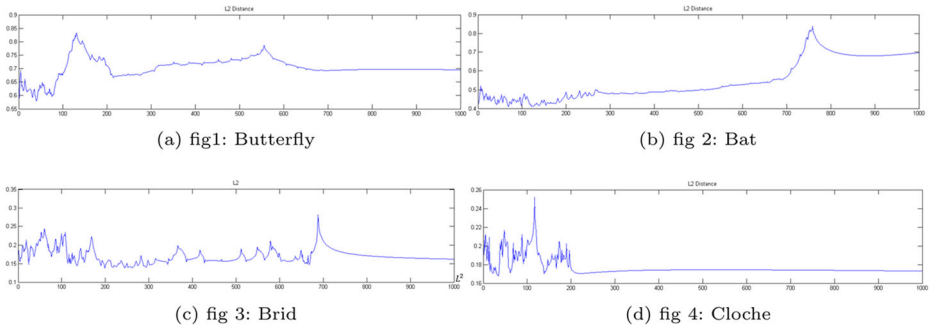
The workflow of Steps 4,5 is depicted in comprehensive detail in Fig. 3.

Figure 4 illustrates the acquired set  $S$  of distances with a minimum value of  $\min L^2_{\sigma_k}$ . For each different shape, each subfigure represents the minimum  $\min L^2_{\sigma_k}$  that can be achieved depending on the value of  $\sigma_k$ . However, when we smooth the normalized input contours using a Gaussian kernel with an increasing standard deviation, the shape starts to lose information at a certain level (becomes an ellipse). This leads us to select the sigma that has a smaller  $\min L^2_{\sigma_k}$  distances.

### 4.2 Part B: unsupervised Bayesian classification

Part B describes the process of unsupervised Bayesian classification to choose the optimal scale levels for the registration. In the following, we detail each step separately.





**Fig. 4**  $\min L^2_{\sigma_k}$  distance variation depending on  $\sigma_k$

**Input:** - Vector  $S = \min L^2_{\sigma_k}$ .  
 -  $k =$  number of clusters.

**Output:**  $K$  optimal classes using the SSE criterion.

**Step1:** For each cluster, an initial clustering center is determined.

**Step2:** The sample-set is assigned to nearest neighbor clustering using the minimum distance principle.

**Step3:** Using each cluster’s mean as a new clustering center.

**Step4:** Steps 2 and 3 should be repeated until the cluster center is no longer changing.

**Algorithm 1** K-means.

- B-1: Applying K-means: It is commonly known that the K-means algorithm [49] requires a large initial set to start clustering. As a result, the K-means approach is preferred for many clustering tasks, especially those involving small datasets. On the other hand, the unsupervised clustering process of K-Means needs fewer iterations and is therefore quicker. In addition, the k-means algorithm has undergone several changes to increase its performance. Algorithm 1 implements K-means unsupervised clustering.

**Calculating the SSE distance:**

The Sum of Squared Errors (SSE) is the sum of the average Euclidean Distance of each point from the centroid.

$$SSE = \sum_{i=1}^n d^2 \tag{14}$$

$d$ : is the distance between the data and the cluster center

- B-2: Visualization of the Elbow graph: The elbow method [74] is presented to explain and evaluate the consistency of clustering analysis to assist in choosing the correct number of clusters that should be present in the data set. This technique is referred to as an optimal clustering technique. In order to initiate the Binary-EM, we have decided to use this illustrated method in order to find the ideal amount of classes to use. Figure 5 demonstrates the use of the Elbow method in the Brid class of shapes.
- B-3: Choosing the best classes ‘K’: The graph is used to determine the class number. A class is actually represented by each Elbow. The optimal  $K$  class number is then the graph-derived number.

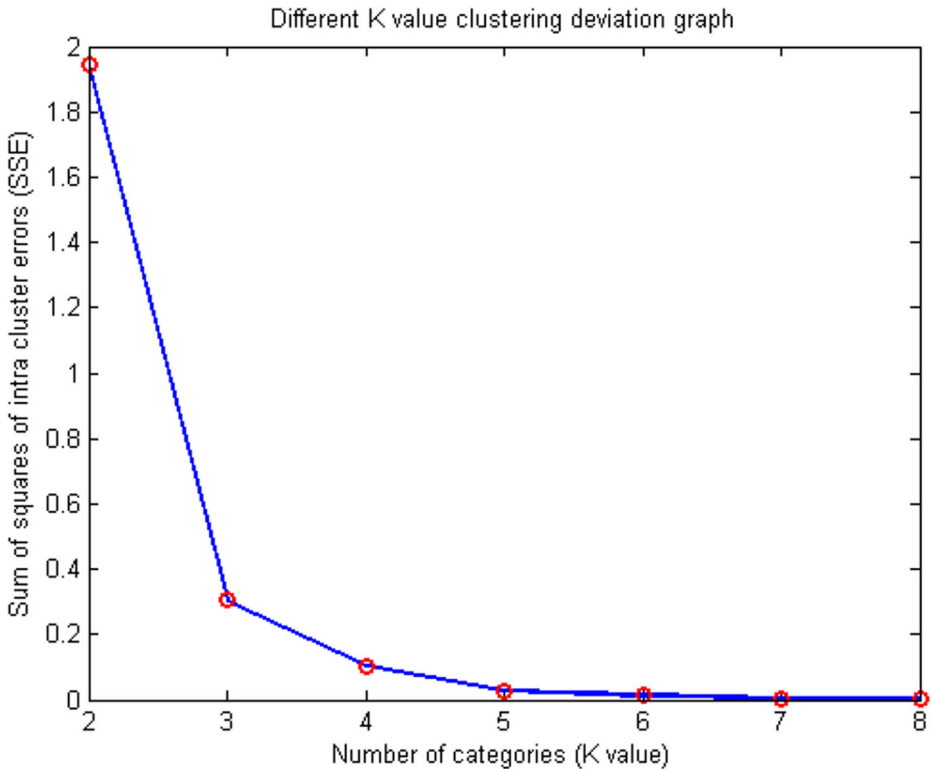
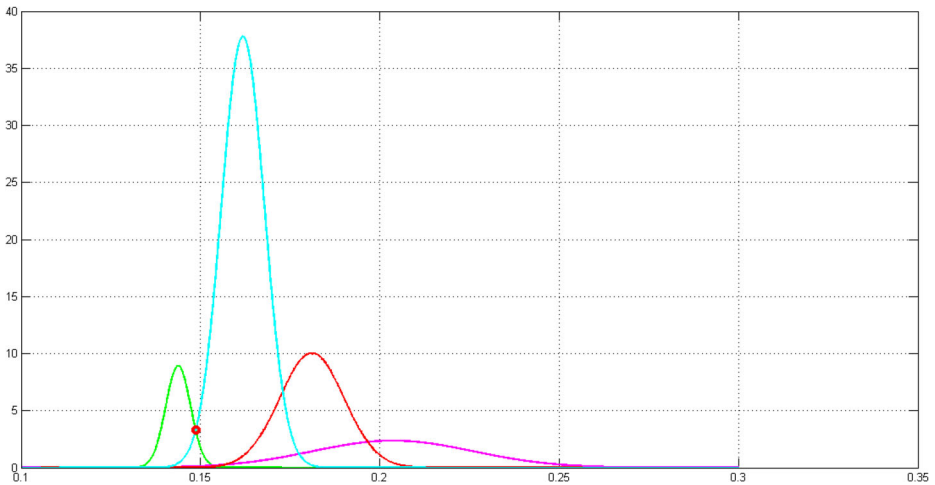


Fig. 5 Example of Elbow method visualization for Brid class of shapes

- B-4: Applying the Multiclass-EM: The algorithm employs an iterative process to determine the probability distribution parameters with the highest likelihood of its attributes. We use EM based on Gaussian mixture models (GMM) for this approach.
  - The input parameters of Multiclass-EM are the set  $S$  of all values of  $\{\min L_{\sigma_i}^2(1 \leq i \leq p)\}$ .
  - $K$  is the number of clusters estimated by the Elbow method. (optimally chosen from Elbow plot)
  - The output is presented in Fig. 6.
- B-5: Bayes Classification: The new threshold  $s_0$  is deduced after the application of the Bayesian rule, as shown in Fig. 6. Thus we obtain  $S^* = \{\sigma_k = \arg \min L_{\sigma_k}^2(1 \leq k \leq p) / L_{\sigma_k}^2 \leq s_0\}$ , let denoted  $q = \text{Card}(S^*)$ .
- B-6: we select only the scale levels belonging to  $S^*$ , which we are denoted by  $\sigma_{j(1 \leq j \leq q)}$ .
- B-7: The registration is done with our new approach Affine Multi-scale Curve Registration (AMSCR) based on unsupervised Bayesian classification.

The procedure of our Affine Multi-scale Curve Registration (AMSCR) based on unsupervised Bayesian classification is described in Algorithm 2.



**Fig. 6** Calculate the new threshold  $s'_0$  using Bayesian Rule

---

**Step1:** Take two Extracted contours.

**Step2:** A multi-scale affine re-parametrization .

**Step2.1:** Re-parametrize the two contours by Affine length  $f^*$  and  $h^*$ .

**Step2.2:** Smooth the two contours using a Gaussian kernel with an increasing standard deviation.

**Step3:** Apply the ACM algorithm

**Step4:** Estimate the euclidean distance  $L_2$  for each smoothed level.

**Step5:** Use K-means for unsupervised clustering.

**Step6:** Calculate the SSE distance.

**Step7:** Apply the visualized Elbow method to choose the optimal K clusters.

**Step8:** Apply Multiclass-EM to select the optimal smoothed levels.

**Step9:** Use these relevant scales to predict registration parameters.

---

**Algorithm 2** AMSCR based on unsupervised Bayesian classification.

Figure 7 presents a comparison of the resulting registration using different approaches. Hence, in the first column, the registration is done by the Affine Multi-scale Curve Registration (AMSCR) [64], in the second column, the alignment is achieved using the adjusted Affine Multi-scale Curve Registration (AMSCR) with Binary-EM [64]. Finally, we use the optimized AMSCR based on Multiclass-EM to do the registration in the third one. As we constat, the optimized AMSCR algorithm Multiclass-EM gives us the best alignment compared to the two other registered shapes.

## 5 Experiments

The proposed method is tested on well-known datasets such as MPEG-7, Multiview Curve Dataset (MCD), Kimia-99, Kimia-216, ETH-80, and the Swedish leaf dataset. So, we test the performance of the optimized AMSCR based on unsupervised Bayesian Classification.

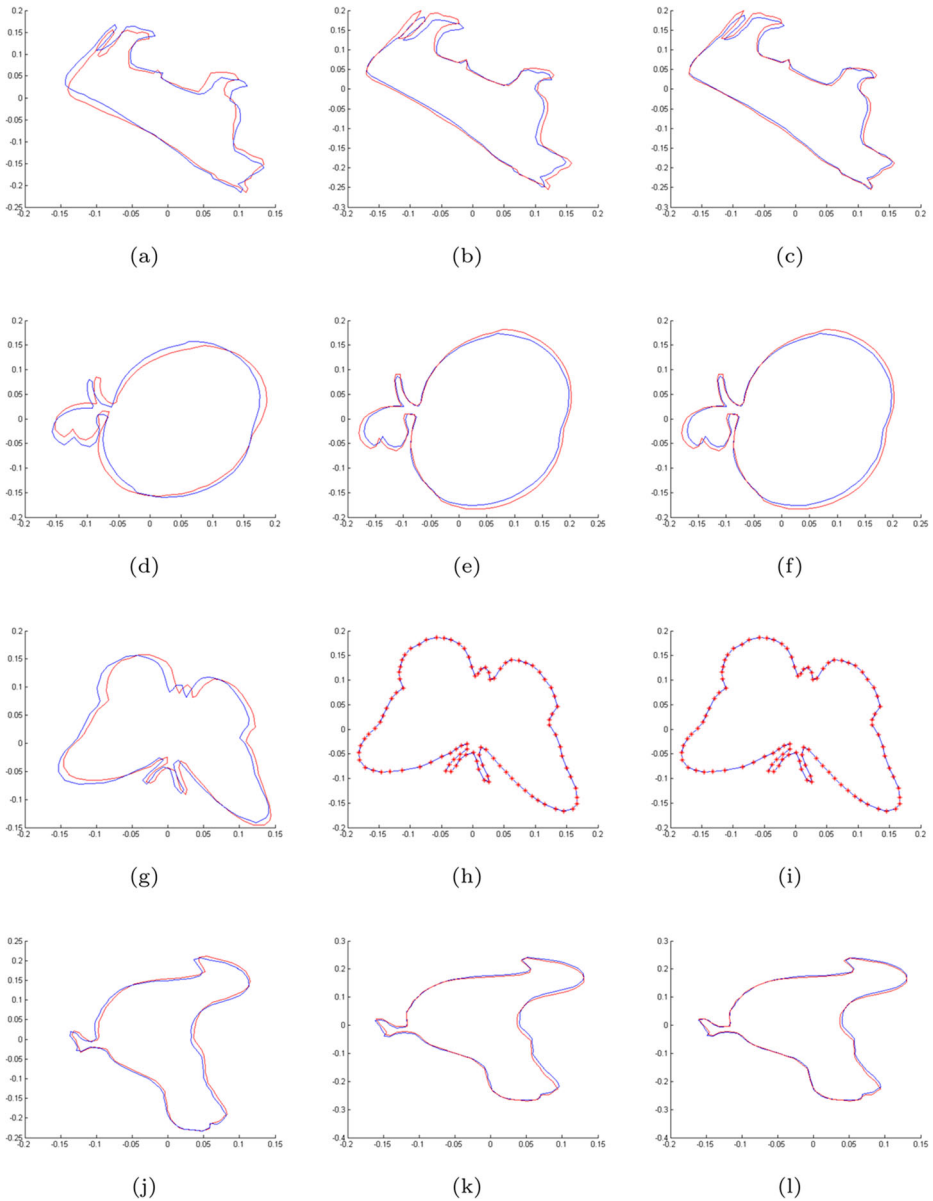


**Fig. 7** a,d,g,j: registration using AMSCR method [64]; b,e,h,k: registration using AMSCR with Binary-EM [64]; c,f,i,l: registration using AMSCR optimized with Multiclass-EM

The comparison is made to the existing shape alignment methods in the stat-of-art. The outcomes of the various methods for these datasets are derived from their respective articles. Furthermore, the evaluation is conducted under the same conditions as the other methods.

MATLAB was used to implement the entire algorithm. And for the resampling conditioning, we use the parameterization according to the study done in [19].

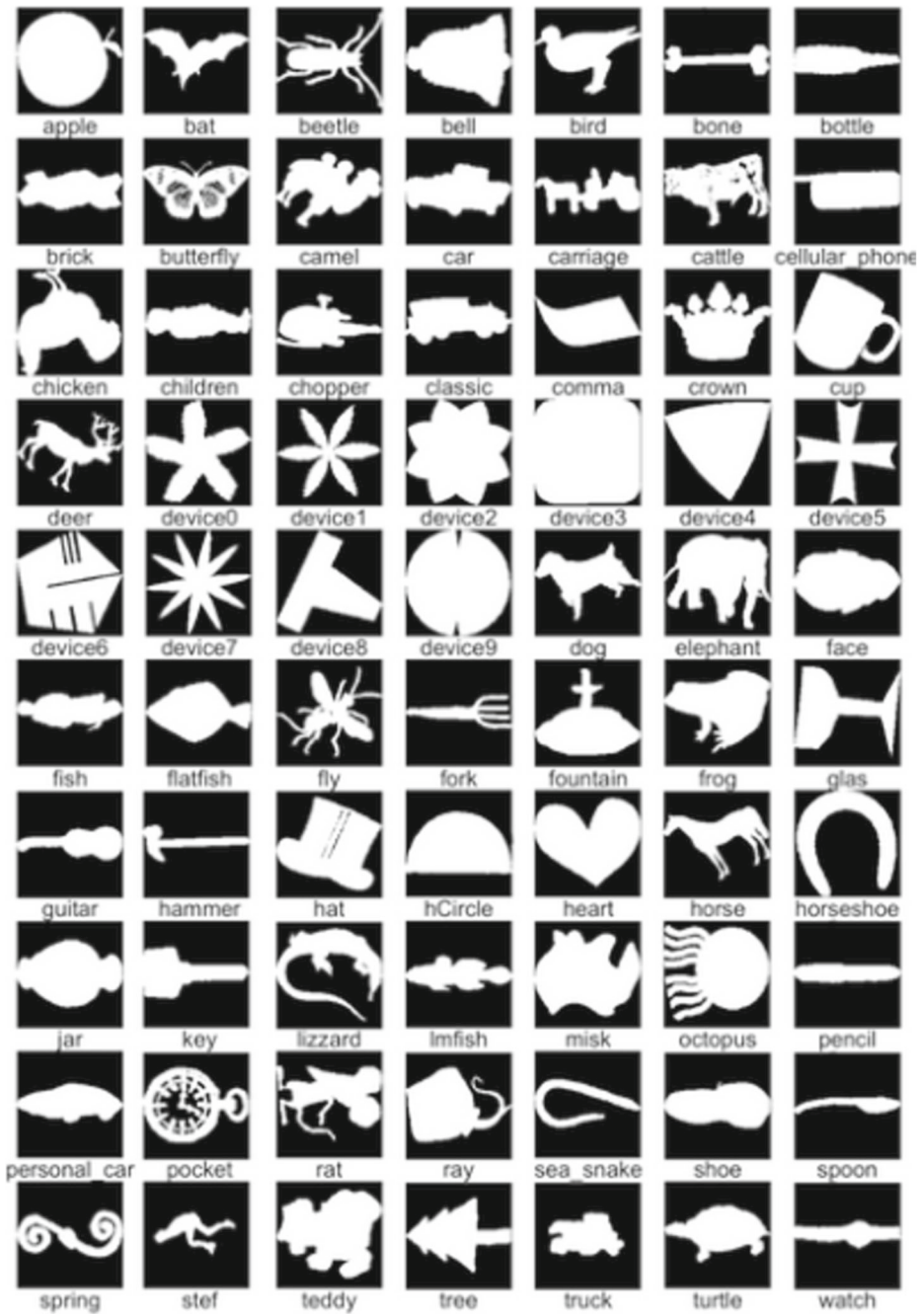


Fig. 8 MPEG7 Dataset

## 5.1 MPEG-7 Image database retrieval

The MPEG-7 shape database [42] is divided into two categories based on shape variations: Set-A and Set-B. The MPEG-7 set-A contains rigid objects with some transformations such as rotations or scale invariance, defined by 840 shapes from 140 classes. The MPEG-7 set-B, represented by 1400 shapes classified into 70 classes, is used for similarity-based retrieval and shape descriptor robustness under various arbitrary shape distortions. Set-B is divided into two parts, Set-B1 and Set-B2, for articulations and missing or altered contour portions, respectively. Figure 8 depicts some examples from each category. To put the proposed approaches to the test in the shape retrieval task, we compute the bull's eye rates defined in [4, 78, 91]. The first step is to compare each curve to the whole dataset curves and recover the number of the same class contour in the middle of the  $2N_c$  most similar, with  $N_c$  being the sample number per class. Then, we calculate the ratio of the number of correct results and the highest possible number of right results [24].

Table 1 covers the Bull's Eye scores of the proposed algorithms with the existing methods. We note that the ACM algorithm [21] 91.55% outperformed the other registration methods proposed in the literature in terms of bull's eye score, such as Fast and non-rigid global registration [20] 82.42%, Multiscale Fourier descriptor [86] 83.94%, AICD [24] 84.26%, MSFDGF-SH [97] 87.76%, IDSC + AspectNorm + SR [73] 88.39%, Invariant multi-scale [84] 91.25% and IMTF [87] 91.26%. Whereas, IDSC + LCDP [88] 93.32%, IDSC + Affine Normlization [28] 93.67%, and Invariant multi-scale + LP [84] 94.51% achieve a high retrieval performance scores compared to the ACM algorithm. For this,

**Table 1** Retrieval results on the entire MPEG-7 set B dataset

Algorithm	Bull's eye score
Multi-scale contour flexibility shape signature [69]	67.57%
Shape Contexts [4]	76.51%
GCSS [5]	78.84%
SMR by data-driven EM [76]	80.03%
Affine CSS [52]	81.12%
CSS-SW [50]	81.33%
Fast and non-rigid global registration [20]	82.42%
AICD [24]	84.26%
Multiscale Representation [1]	84.93%
IDSC + AspectNorm + SR [73]	88.39%
Multiscale Fourier descriptor [86]	83.94%
MSFDGF-SH [97]	87.76%
Invariant multi-scale [84]	91.25%
IMTF [87]	91.26%
ACMA[19]	91.55%
IDSC + LCDP [88]	93.32%
AMSCR [64]	93.61%
IDSC + Affine Normlization [28]	93.67%
AMSCR using Binary-EM [64]	94.36%
AMSCR based on Multiclass-EM	94.49%
Invariant multi-scale + LP [84]	94.51%

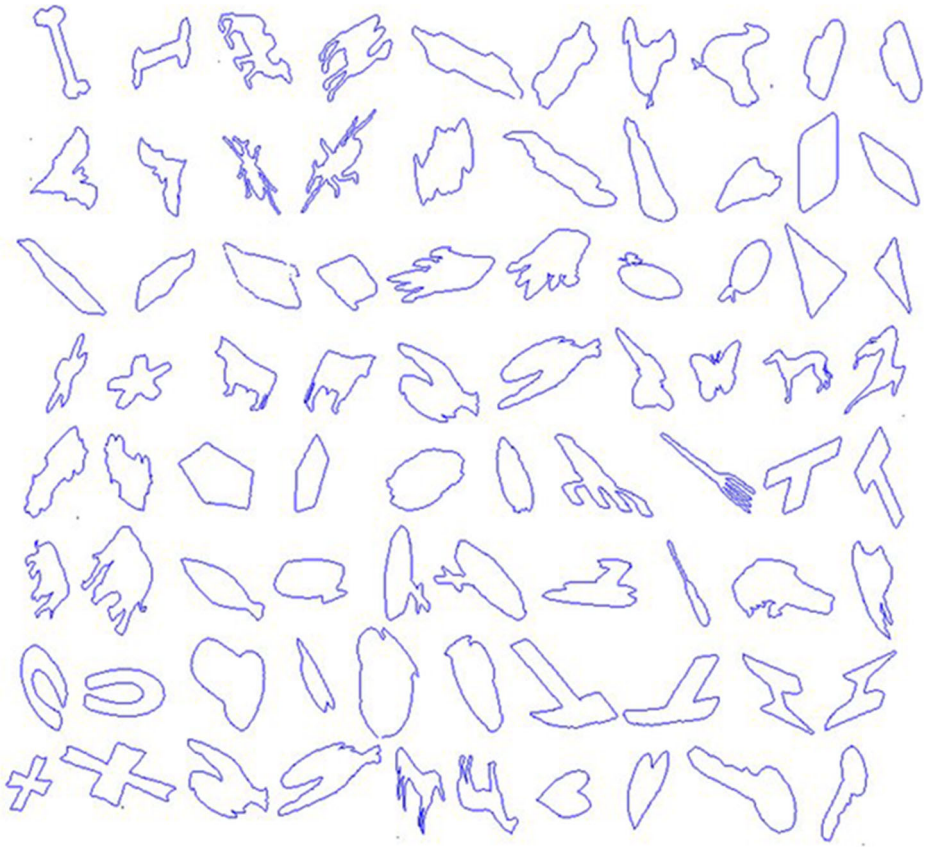


**Fig. 9** Different shape images from the MCD dataset, two images from each class

we implemented several steps to enhance these results in this paper, starting with Affine Multi-Scale Curve Registration (AMSCR), which improves the ACMA bull’s eye score

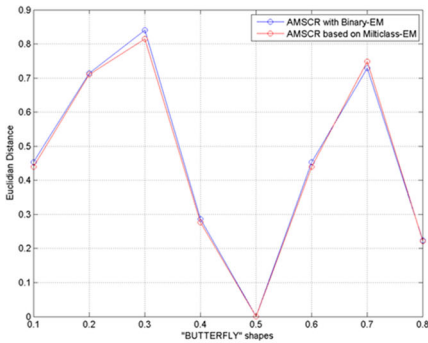
**Table 2** Retrieval results on the entire MCD dataset

Methods	Average
Arber [2]	41%
SC [55]	56.29%
Huang [34]	71%
Rube [16]	79%
Mai [50]	89%
Fast and non-rigid global registration [20]	92.8%
ACMA [19]	94%
Partial Contour Matching Based on ACSS [21]	95.98%
AMSCR [64]	96.36%
AMSCR with Binary-EM [64]	96.58%
AMSCR with Multiclass-EM	96.61%

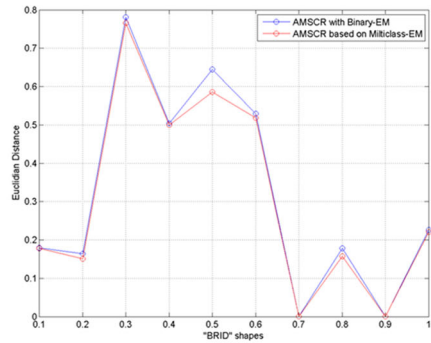
by 2.06%. Then, the result becomes even better when we adjusted the Affine Multi-Scale Curve Registration (AMSCR) with Binary-EM, which improves the AMSCR algorithm score by 0.75%. Moreover, when we optimize the proposed AMSCR with Multiclass-EM, the results become more competitive, where this one outperformed AMSCR with Binary-EM by 0.12%. On the other hand, the method Invariant multi-scale + LP [84] remains more efficient than our suggested AMSCR with Multiclass-EM by 0.03%.

### 5.2 MCD image database retrieval

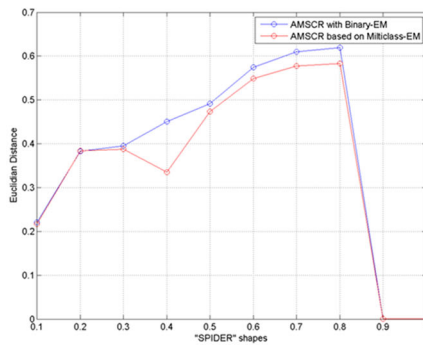
Shape registration is one of the most significant applications of the algorithm proposed. Thus, we are going to test the Affine Multi-Scale Curve Registration (AMSCR) [64] and the optimized AMSCR based on Multiclass-EM on the Multiview Curve Dataset (MCD) [98] which is composed of 40 shape classes taken from the MPEG-7 database. Each category contains 14 sample curves that match the distortion of the original curve from a different perspective Fig. 9. Table 2 compares our proposed methods and some existing work in state-of-the-art. First, we noticed that the Affine Multi-Scale Curve Registration (AMSCR)



(a) Butterfly class



(b) Brid class



(c) Spider class

**Fig. 10** Computation of the Euclidian Distance between two shapes: the blue curve represents the  $L_2$  distance using the adjusted AMSCR with Binary-EM. The red one describes the same  $L_2$  using the optimized AMSCR based on Multiclass-EM



96.36% exceeds the other registration techniques such as the methods Partial Contour Matching Based on ACSS [52] 95.98%, ACMA [19] 94%, Fast and non-rigid global registration [20] 92.8%, Mai [50] 89% and Rube [16] 79%. Then the result becomes better when we adjust the AMSCR with Binary-EM [64], and we obtain 96.58% as a rate. Moreover, the optimized AMSCR based on Multiclass-EM performs substantially more than the other techniques with a 96.61% rate.

### 5.3 Euclidian distance ( $L_2$ ) Computation

Figure 10 shows some graphics obtained from the Euclidian Distance ( $L_2$ ) computation. From the MCD database, we take shape as a query and register it with another shape that belongs to the same class of shapes. Then we calculate the  $L_2$  distance between them using the two approaches, the AMSCR adjusted with Binary-EM and the optimized AMSCR based on Multiclass-EM. The first subfigure (a) compares the Butterfly's  $L_2$  distance, done with the AMSCR with Binary-EM and the AMSCR based on Multiclass-EM. However, we note that the AMSCR based on Multiclass-EM improves the Euclidian Distance in most cases. In the second subfigure (b), we can see that using the optimized AMSCR based on Multiclass-EM improves the computation of  $L_2$  distance for a Bird form significantly. Finally, the new optimized AMSCR based on Multiclass-EM performs well with the Spider shape in the majority of cases.

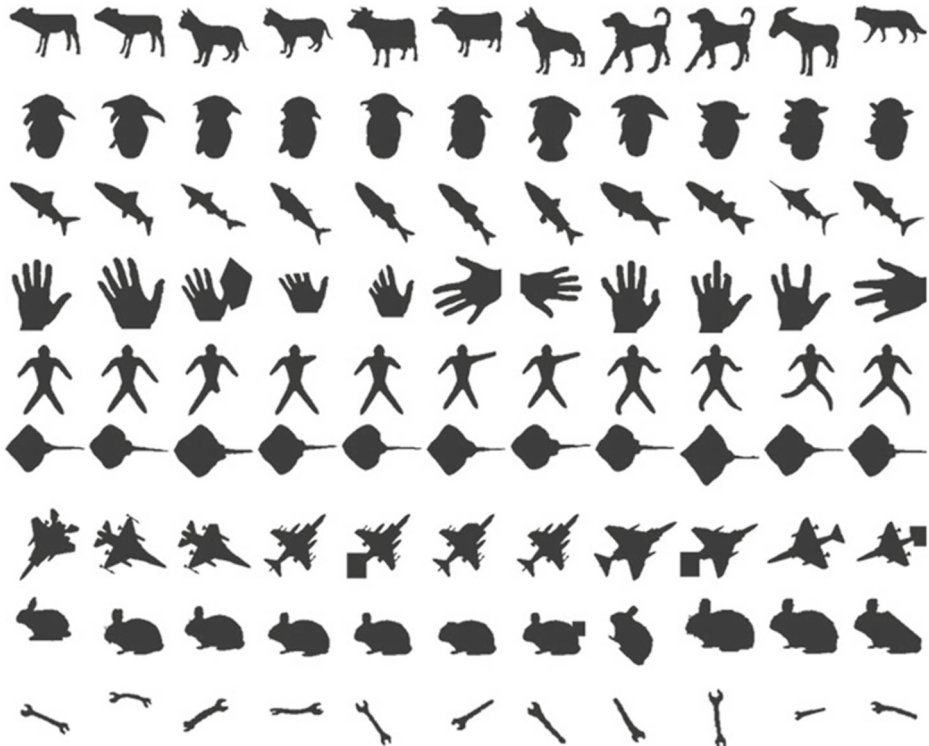


Fig. 11 Kimia-99 database, where each row shows a different class

## 5.4 KIMIA-99 image database retrieval

In shape registration and retrieval, the Kimia-99 dataset [65] is commonly used for evaluation. There are 99 shapes in 9 classes, with 11 in each category (Fig. 11). This dataset contains certain occlusions and articulations. Table 3 displays various well-known methods as a retrieval rate of the top-1 to top-10 alignment shapes. For each of them, the best possible result is 99. The results show that the Affine Multi-Scale Curve Registration (AMSCR) [64] outperforms other approaches. However, the adjusted AMSCR with Binary-EM [64] and the optimized AMSCR based on Multiclass-EM perform very similarly and give competitive results compared to the most existing methods such as Generative model [75], HF [79], IDSC+LBP [67], ACMA [19], and SMR by data-driven EM [76].

## 5.5 KIMIA-216 image database retrieval

The Kimia-216 dataset [65] is made up of 216 curves divided into 18 classes, each one with 12 shapes. Figure 12 illustrates all 216 forms in this database, each in a column belonging to a class. Columns depict birds, bones, bricks, camels, cars, children, classic cars, elephants, faces, forks, fountains, glass, hammers, hearts, keys, misks, rays, and turtles from left to right. The Affine Multi-Scale Curve Registration (AMSCR) [64] is tested first, followed by the AMSCR adjusted with Binary-EM [64] and the optimized AMSCR based on Multiclass-EM. The outcomes demonstrate that the proposed algorithm exceeds other techniques such

**Table 3** Top 10 closest matching shapes for Kimia-99 dataset

Algorithm	Top1	Top2	Top3	Top4	Top5	Top6	Top7	Top8	Top9	Top10
Shape context [4]	97	91	88	85	84	77	75	66	56	37
CPDH+EMD(eucl) [68]	96	94	94	87	88	82	80	70	62	55
CPDH+EMD(shift) [68]	98	94	95	92	90	88	85	84	71	52
Generative model [75]	99	97	99	98	96	96	94	83	75	48
PS+LBP [25]	99	97	97	88	88	86	86	90	80	77
Shock graphs [65]	99	99	99	98	98	97	96	95	93	82
MDS+SC+DP [45]	99	98	98	98	97	99	97	96	97	85
IDSC+DP [45]	99	99	99	98	98	97	97	98	94	79
Shock Edit [65]	99	99	99	98	98	98	96	95	94	86
Shape-tree [23]	99	99	99	99	99	99	99	97	93	86
GM [15]	99	99	99	99	99	99	99	97	93	86
Symbolic rep [13]	99	99	99	99	96	96	99	95	93	88
IMC [89]	99	99	99	99	98	97	95	94	90	83
HF [79]	99	99	99	99	98	99	99	96	95	88
IDSC+LBP [67]	99	99	99	99	98	97	97	98	98	96
ACMA [19]	99	99	99	99	99	99	98	98	97	95
SMR by data-driven EM [76]	99	97	99	98	96	96	94	83	75	48
AMSCR [64]	99	99	99	99	99	99	98	98	97	96
AMSCR with Binary-EM [64]	99	99	99	99	99	99	96	98	98	96
AMSCR based on Multiclass-EM	99	99	99	99	99	99	98	97	98	97



**Fig. 12** Example of curves in Kimia-216 database. One object for each one of the 18 categories is shown

as CPDH+EMD(eucl) [68], CPDH+EMD(shift) [68], PS+LBP [26], IDSC+LBP [79], even the ACMA [19] method (Table 4).

## 5.6 ETH-80 image database retrieval

ETH-80 benchmark contains 3280 images. It is divided into eight classes. Each class includes ten objects containing 41 images obtained from various poses. Figure 13 depicts some examples from the ETH-80 dataset [43]. To classify the different categories in the experiment, we use the 1-nearest neighbor algorithm. Each image is compared to the other 79 images in the same category to determine the recognition rate. Table 3 shows the accuracy of the proposed approaches with other existing methods. We notice that the Affine Multi-Scale Curve Registration (AMSCR) [64] has a rate equal to 88.98%. However, when we adjusted AMSCR with Binary-EM [64], the accuracy increased by 0.25%. The result improved by 89.45% when the AMSCR has optimized with Multiclass-EM. Our approach gives better accuracy compared to other existing techniques such as Multiscale Fourier descriptor [86] (86.91%), EGCSS [5](87.5%), Fast and non-rigid global registration [20]

**Table 4** Top 11 closest matching shapes for Kimia-216 dataset

Algorithm	Top1	Top2	Top3	Top4	Top5	Top6	Top7	Top8	Top9	Top10	Top11
Shape context [4]	214	209	205	197	191	178	161	144	131	101	78
CPDH+EMD(eucl) [68]	214	215	209	204	200	193	187	180	168	146	114
CPDH+EMD(shift) [68]	215	215	213	205	203	204	190	180	168	154	123
PS+LBP [26]	216	209	205	195	195	197	188	180	179	163	152
HF [79]	216	216	216	215	215	212	211	204	200	194	179
IDSC+LBP [79]	216	215	216	214	213	215	215	213	210	207	204
ACMA [19]	216	216	216	216	215	216	214	213	212	206	206
AMSCR [64]	216	216	216	216	215	216	213	213	212	206	204
AMSCR with [64] Binary-EM	216	216	216	216	214	216	214	213	210	207	206
AMSCR based on Multiclass-EM	216	216	216	216	215	216	215	214	212	207	207

(87.95%) and Height function [79] (88.72%). However, our method's accuracy is inferior to that of the deep learning method for hierarchical features based on CNN [39] (95.80%) (Table 5).

## 5.7 Swedish leaf dataset

This section evaluates our proposed method in the Swedish leaf dataset. This benchmark contains 1125 objects from 15 different leaf categories. As illustrated in Fig. 14, each class

**Fig. 13** ETH-80 database

**Table 5** Retrieval rates on the entire ETH-80 dataset

Methods	Score
Combined perimeter area function FD [94]	75.52%
Normalized complex coordinate FD [71]	76.34%
PCA gray [34]	82.99%
MDS+SC+DP [45]	86.80%
Multiscale Fourier descriptor [86]	86.91%
EGCSS [5]	87.50%
Fast and non-rigid global registration [20]	87.95%
IDSC+DP [45]	88.11%
Height function [79]	88.72%
AMSCR [64]	88.98%
AMSCR with Binary-EM [64]	89.13%
AMSCR based on Multiclass-EM	89.45%
Hierarchical feature using CNN [39]	95.80%

**Fig. 14** Swedish leaf dataset

**Table 6** Retrieval rates on the entire Swedish leaf dataset

Methods	Score
Normalized complex coordinate FD [71]	94.53%
MSFDGF-SH-DS+MD [97]	95.47%
Multiscale Fourier descriptor [86]	86.91%
Fast and non-rigid global registration [20]	95.61%
Shape tree [23]	96.28%
AMSCR [64]	96.3%
EGCSS [5]	97.07%
AMSCR with Binary-EM [64]	96.51%
AMSCR based on Multiclass-EM	96.73%
HSC [78]	96.91 %
IMTF [87]	97.87%

includes 75 forms. This dataset contains forms of the same category with significant variability and shapes belonging to a diverse category that can be very similar. We evaluate the performances in the same state indicated in [70] to compare the proposed method with state-of-the-art. We choose 25 learning objects randomly from each category, and the remaining objects serve as a test. The sample object is then aligned with the training objects. The shape will be classified using the 1-nearest neighbor and the distance L2 following registration. Table 6 summarizes the accuracy rates. The method Affine Multi-Scale Curve Registration (AMSCR) [64] gives us a score equal to 96.3% which is better than several other techniques such as Multiscale Fourier descriptor [86] (86.91%), Fast and non-rigid global registration [20] (95.61%). Moreover, the adjusted AMSCR with Binary-EM [64] enhance the result by 96.51%, and the score is better when the AMSCR optimized by Multiclass-EM (96.73%). Contrariwise, there are some other methods in the state of the art that give better rates such as HSC [78] (96.91%) and IMTF [87] (97.87%).

**Table 7** Efficiency of different methods on the MPEG-7 dataset

Methods	Time (s)
Combined perimeter area function FD [94]	601
Invariant curvature-based Fourier shape descriptors [18]	547
Triangle centroid area FD [93]	25
Centroid distance FD [94]	25
Farthest point distance FD [17]	28
Normalized complex coordinate FD [71]	26
ACMA [19]	29
MFD [86]	33
Fast and non-rigid global registration [20]	30
Height function MTCD [90]	39
AMSCR based on Multiclass-EM	31
Invariant curvature-based [79]	17,139
IDSC+DP [45]	10,929

## 6 Analysis of time consumption

The effectiveness of our proposed approach is compared with those of other methods. Shape smoothing and normalization time are not considered while estimating time consumption. According to [86], the suggested method's time consumption is identical to that of the other approaches. Table 7 shows that for MPEG-7 datasets, the proposed process takes 31 s, encouraging the use of our method in real-time applications.

## 7 Conclusion

In this paper, we have proposed an optimized Affine Multi-Scale Curve Registration (AMSCR) based on the multiclass-EM algorithm. This method's main idea is to automatically select the best set of smoothing parameters in the sense of the minimum of the Euclidean distance between the target and the source curves.

Thus, we have obtained a global rectangular linear system corresponding to this selected set of their smoothed parameters. The number of the class is founded by the application of the k-means and Elbow method. The registration process is achieved by the application of the pseudo-inverse algorithm.

Based on several experiments on MPEG-7, MCD, Kimia-99, Kimia216, ETH-80, and the Swedish leaf benchmarks, we have proven that the proposed method gives one of the best scores in the mean of precision. We aim, in future works, to study the stability and the complexity of our registration system. And we intend to improve the gigantic stitching mosaic done for the virtual Tunisian Bardo Museum.

**Data Availability** Data sharing not applicable to this article as no datasets were generated or analyzed during the current study.

### Declarations

**Conflict of Interests** The authors declare that they have no conflict of interest.

## References

1. Adamek T, O'Connor NE (2004) A multiscale representation method for nonrigid shapes with a single closed contour. *IEEE Trans Circuits Syst Video Technol* 14(5):742–753
2. Arbter K, Snyder WE, Burkhardt H, Hirzinger G (1990) Application of affine-invariant fourier descriptors to recognition of 3-d objects. *IEEE Trans Pattern Anal Mach Intell* 12(7):640–647
3. Bacheider IA, Ullman S (1992) Contour matching using local affine transformations. Technical report Massachusetts Inst of Tech Cambridge Artificial Intelligence Lab
4. Belongie S, Malik J, Puzicha J (2002) Shape matching and object recognition using shape contexts. *IEEE Trans Pattern Anal Mach Intell* 24(4):509–522
5. BenKhelifa A, Ghorbel F (2019) An almost complete curvature scale space representation: Euclidean case. *Signal Process Image Commun* 75:32–43
6. Besl PJ, McKay ND (1992) Method for registration of 3-d shapes. In: *Sensor fusion IV: control paradigms and data structures*, vol 1611. International Society for Optics and Photonics, pp 586–606
7. Bryner D, Srivastava A, Klassen E (2012) Affine-invariant, elastic shape analysis of planar contours. In: 2012 IEEE conference on computer vision and pattern recognition, IEEE, pp 390–397
8. Bryner D, Srivastava A (2014) Bayesian active contours with affine-invariant, elastic shape prior. In: *Proceedings of the IEEE conference on computer vision and pattern recognition*, pp 312–319

9. Chui H, Rangarajan A (2000) A feature registration framework using mixture models. In: Proceedings IEEE workshop on mathematical methods in biomedical image analysis. MMBIA-2000 (Cat. No. PR00737), IEEE, pp 190–197
10. Chui H, Rangarajan A (2003) A new point matching algorithm for non-rigid registration. *Comput Vis Image Underst* 89(2-3):114–141
11. Cyganski D, Vaz RF (1992) Linear signal decomposition approach to affine-invariant contour identification. In: Intelligent robots and computer vision x: algorithms and techniques, vol 1607, International Society for Optics and Photonics, pp 98–109
12. Cyganski D, Cott TA, Orr JA, Dodson RJ (1988) Object identification and orientation estimation from contours based on an affine invariant curvature. In: Intelligent robots and computer vision VI, vol 848, International Society for Optics and Photonics, pp 33–39
13. Daliri MR, Torre V (2008) Robust symbolic representation for shape recognition and retrieval. *Pattern Recognit* 41(5):1782–1798
14. Dempster AP, Laird NM, Rubin DB (1977) Maximum likelihood from incomplete data via the em algorithm. *J R Stat Soc Ser B Stat (Methodol)* 39(1):1–22
15. Egozi A, Keller Y, Guterman H (2010) Improving shape retrieval by spectral matching and meta similarity. *IEEE Trans Image Process* 19(5):1319–1327
16. El Rube I, Ahmed M, Kamel M (2005) Wavelet approximation-based affine invariant shape representation functions. *IEEE Trans Pattern Anal Mach Intell* 28(2):323–327
17. El-ghazal A, Basir O, Belkasim S (2009) Farthest point distance: a new shape signature for fourier descriptors. *Signal Process Image Commun* 24(7):572–586
18. El-ghazal A, Basir O, Belkasim S (2012) Invariant curvature-based fourier shape descriptors. *J Vis Commun Image Represent* 23(4):622–633
19. Elghoul S, Ghorbel F (2021) A fast and robust affine-invariant method for shape registration under partial occlusion. *Int J Multimed Inf Retr* 1–21
20. Elghoul S, Ghorbel F (2021) Fast global sa (2, r) shape registration based on invertible invariant descriptor. *Signal Process Image Commun* 90:116058
21. Elghoul S, Ghorbel F (2021) Partial contour matching based on affine curvature scale space descriptors. In: New approaches for multidimensional signal processing: proceedings of international workshop, NAMSP 2020, vol 216, Springer, p 73
22. Ersi EF, Zelek JS (2006) Local feature matching for face recognition. In: The 3rd Canadian conference on computer and robot vision (CRV'06), IEEE, pp 4–4
23. Felzenszwalb PF, Schwartz JD (2007) Hierarchical matching of deformable shapes. In: 2007 IEEE Conference on computer vision and pattern recognition, IEEE, pp 1–8
24. Fu H, Tian Z, Ran M, Fan M (2013) Novel affine-invariant curve descriptor for curve matching and occluded object recognition. *IET Comput Vis* 7(4):279–292
25. Genovese A, Piuri V, Scotti F (2014) Touchless palmprint recognition systems, vol 60. Springer
26. Genovese A, Piuri V, Scotti F (2014) Palmprint biometrics. In: Touchless palmprint recognition systems, Springer, pp 49–109
27. Ghorbel F, Daoudi M, Mokadem A, Avaro O, Sanson H (1996) Global planar rigid motion estimation applied to object-oriented coding. In: Proceedings of 13th international conference on pattern recognition, vol 2, IEEE, pp 641–645
28. Gopalan R, Turaga P, Chellappa R (2010) Articulation-invariant representation of non-planar shapes. In: European conference on computer vision, Springer, pp 286–299
29. Gope C, Kehtarnavaz N, Hillman G, Würsig B (2005) An affine invariant curve matching method for photo-identification of marine mammals. *Pattern Recogn* 38(1):125–132
30. Granger S, Pennec X (2002) Multi-scale em-icp: a fast and robust approach for surface registration. In: European conference on computer vision, Springer, pp 418–432
31. Hemamalini G, Prakash J (2016) Medical image analysis of image segmentation and registration techniques. *Int J Eng Technol (IJET)* 8(5):2234–2241
32. Hu M-K (1962) Visual pattern recognition by moment invariants. *IEEE Trans Inf Theory* 8(2):179–187
33. Hu R, Jia W, Ling H, Huang D (2012) Multiscale distance matrix for fast plant leaf recognition. *IEEE Trans Image Process* 21(11):4667–4672
34. Huang X, Wang B, Zhang L (2005) A new scheme for extraction of affine invariant descriptor and affine motion estimation based on independent component analysis. *Pattern Recogn Lett* 26(9):1244–1255
35. Huang X, Paragios N, Metaxas DN (2006) Shape registration in implicit spaces using information theory and free form deformations. *IEEE Trans Pattern Anal Mach Intell* 28(8):1303–1318
36. Jian B, Vemuri BC (2010) Robust point set registration using gaussian mixture models. *IEEE Trans Pattern Anal Mach Intell* 33(8):1633–1645



37. Kang E-Y, Cohen I, Medioni G (2000) A graph-based global registration for 2d mosaics. In: Proceedings 15th international conference on pattern recognition. ICPR-2000, vol 1, IEEE, pp 257–260
38. Kaothanthong N, Chun J, Tokuyama T (2016) Distance interior ratio: a new shape signature for 2d shape retrieval. *Pattern Recognit Lett* 78:14–21
39. Ke Q, Li Y (2014) Is rotation a nuisance in shape recognition? In: Proceedings of the IEEE conference on computer vision and pattern recognition, pp 4146–4153
40. Kovalsky SZ, Cohen G, Hagege R, Francos JM (2010) Decoupled linear estimation of affine geometric deformations and nonlinear intensity transformations of images. *IEEE Trans Pattern Anal Mach Intell* 32(5):940–946
41. Krotosky SJ, Trivedi MM (2007) Mutual information based registration of multimodal stereo videos for person tracking. *Comput Vis Image Underst* 106(2–3):270–287
42. Latecki LJ, Lakamper R, Eckhardt T (2000) Shape descriptors for non-rigid shapes with a single closed contour. In: Proceedings IEEE conference on computer vision and pattern recognition. CVPR 2000 (Cat. No. PR00662), vol 1, IEEE, pp 424–429
43. Leibe B, Schiele B (2003) Analyzing appearance and contour based methods for object categorization. In: 2003 IEEE Computer society conference on computer vision and pattern recognition, 2003. proceedings, vol 2, IEEE, p 409
44. Lin W-S, Fang C-H (2007) Synthesized affine invariant function for 2d shape recognition. *Pattern Recogn* 40(7):1921–1928
45. Ling H, Jacobs DW (2007) Shape classification using the inner-distance. *IEEE Trans Pattern Anal Mach Intell* 29(2):286–299
46. Liu H (2014) Curves in affine and semi-euclidean spaces. *RM* 65(1):235–249
47. Liu C, Kong X, Zhao X (2020) Non-rigid point set registration based on new shape context and local structure constraint. In: Proceedings of the 2020 9th international conference on computing and pattern recognition, pp 439–446
48. Ma J, Zhao J, Tian J, Tu Z, Yuille AL (2013) Robust estimation of nonrigid transformation for point set registration. In: Proceedings of the IEEE conference on computer vision and pattern recognition, pp 2147–2154
49. MacQueen J et al (1967) Some methods for classification and analysis of multivariate observations. In: Proceedings of the fifth Berkeley symposium on mathematical statistics and probability, vol 1, Oakland, pp 281–297
50. Mai F, Chang C, Hung Y (2010) Affine-invariant shape matching and recognition under partial occlusion. In: 2010 IEEE international conference on image processing, IEEE, pp 4605–4608
51. Matuk J, Bharath K, Chkrebti O, Kurtek S (2021) Bayesian framework for simultaneous registration and estimation of noisy, sparse, and fragmented functional data. *J Am Stat Assoc* 1–17
52. Mokhtarian F, Abbasi S (2001) Affine curvature scale space with affine length parametrisation. *Pattern Anal Appl* 4(1):1–8
53. Moons T, Pauwels EJ, Van Gool L, Oosterlinck A (1995) Foundations of semi-differential invariants. *Int J Comput Vis* 14(1):25–47
54. Morel J-M, Yu G (2009) Asift: a new framework for fully affine invariant image comparison. *SIAM J Imaging Sci* 2(2):438–469
55. Mori G, Belongie S, Malik J (2005) Efficient shape matching using shape contexts. *IEEE Trans Pattern Anal Mach Intell* 27(11):1832–1837
56. Myronenko A, Song X (2010) Point set registration: coherent point drift. *IEEE Trans Pattern Anal Mach Intell* 32(12):2262–2275
57. Opelt A, Pinz A, Zisserman A (2006) A boundary-fragment-model for object detection. In: European conference on computer vision, Springer, pp 575–588
58. Pauwels EJ, Moons T, Van Gool L, Kempenaers P, Oosterlinck A (1995) Recognition of planar shapes under affine distortion. *Int J Comput Vis* 14(1):49–65
59. Petrakis EGM, Diplaros A, Milios E (2002) Matching and retrieval of distorted and occluded shapes using dynamic programming. *IEEE Trans Pattern Anal Mach Intell* 24(11):1501–1516
60. Pham N, Helbert D, Bourdon P, Carré P (2018) Spectral graph wavelet based nonrigid image registration. In: 2018 25th IEEE international conference on image processing (ICIP), IEEE, pp 3348–3352
61. Pulli K (1999) Multiview registration for large data sets. In: Second international conference on 3-d digital imaging and modeling (cat. no. pr00062), IEEE, pp 160–168
62. Raviv D, Kimmel R (2015) Affine invariant geometry for non-rigid shapes. *Int J Comput Vis* 111(1):1–11
63. Rusinkiewicz S, Levoy M (2001) Efficient variants of the icp algorithm. In: Proceedings third international conference on 3-D digital imaging and modeling, IEEE, pp 145–152

64. Sakrani K, Elghoul S, Falleh S, Ghorbel F (2021) Sa (2, r) multi-scale contour registration based on em algorithm. In: 2021 International conference on visual communications and image processing (VCIP), IEEE, pp 1–5
65. Sebastian TB, Klein PN, Kimia BB (2004) Recognition of shapes by editing their shock graphs. *IEEE Trans Pattern Anal Mach Intell* 26(5):550–571
66. Sellami M, Ghorbel F (2012) An invariant similarity registration algorithm based on the analytical fourier-mellin transform. In: 2012 Proceedings of the 20th European signal processing conference (EUSIPCO), IEEE, 390–394
67. Shekar B, Pilar B, Kittler J (2015) An unification of inner distance shape context and local binary pattern for shape representation and classification. In: Proceedings of the 2nd international conference on perception and machine intelligence, pp 46–55
68. Shu X, Wu X-J (2011) A novel contour descriptor for 2d shape matching and its application to image retrieval. *Image Vis Comput* 29(4):286–294
69. Shu X, Pan L, Wu X-J (2015) Multi-scale contour flexibility shape signature for fourier descriptor. *J Vis Commun Image Represent* 26:161–167
70. Söderkvist O (2001) Computer vision classification of leaves from Swedish trees
71. Sokic E, Konjicija S (2014) Novel fourier descriptor based on complex coordinates shape signature. In: 2014 12th International workshop on content-based multimedia indexing (CBMI), IEEE, pp 1–4
72. Spivak M (1970) A comprehensive introduction to differential geometry part, vol 2. Publish or Perish, Boston
73. Temlyakov A, Munsell BC, Waggoner JW, Wang S (2010) Two perceptually motivated strategies for shape classification. In: 2010 IEEE Computer society conference on computer vision and pattern recognition, IEEE, pp 2289–2296
74. Thorndike RL (1953) Who belongs in the family. In: *Psychometrika*. Citeseer
75. Tu Z, Yuille AL (2004) Shape matching and recognition—using generative models and informative features. In: European conference on computer vision, Springer, pp 195–209
76. Tu Z, Zheng S, Yuille A (2008) Shape matching and registration by data-driven em. *Comput Vis Image Underst* 109(3):290–304
77. Wang G, Chen Y (2017) Fuzzy correspondences guided gaussian mixture model for point set registration. *Knowl-Based Syst* 136:200–209
78. Wang B, Gao Y (2014) Hierarchical string cuts: a translation, rotation, scale, and mirror invariant descriptor for fast shape retrieval. *IEEE Trans Image Process* 23(9):4101–4111
79. Wang J, Bai X, You X, Liu W, Latecki LJ (2012) Shape matching and classification using height functions. *Pattern Recogn Lett* 33(2):134–143
80. Weiss I (1993) Geometric invariants and object recognition. *Int J Comput* 11263on 10(3):207–231
81. Wiskott L, Krüger N, Kuiger N, Von Der Malsburg C (1997) Face recognition by elastic bunch graph matching. *IEEE Trans Pattern Anal Mach Intell* 19(7):775–779
82. Wolter D, Latecki LJ (2004) Shape matching for robot mapping. In: Pacific rim international conference on artificial intelligence, Springer, pp 693–702
83. Xu H, Yang J, Tang Y, Li Y (2015) A hybrid shape descriptor for object recognition. In: 2015 IEEE International conference on robotics and biomimetics (ROBIO), IEEE, pp 96–101
84. Xu H, Yang J, Yuan J (2016) Invariant multi-scale shape descriptor for object matching and recognition. In: 2016 IEEE International conference on image processing (ICIP), IEEE, pp 644–648
85. Yang B, Chen C (2015) Automatic registration of uav-borne sequent images and lidar data. *ISPRS J Photogramm Remote Sens* 101:262–274
86. Yang C, Yu Q (2019) Multiscale fourier descriptor based on triangular features for shape retrieval. *Signal Process Image Commun* 71:110–119
87. Yang C, Yu Q (2021) Invariant multiscale triangle feature for shape recognition. *Appl Math Comput* 403:126096
88. Yang X, Koknar-Tezel S, Latecki LJ (2009) Locally constrained diffusion process on locally densified distance spaces with applications to shape retrieval. In: 2009 IEEE conference on computer vision and pattern recognition, IEEE, pp 357–364
89. Yang J, Wang H, Yuan J, Li Y, Liu J (2016) Invariant multi-scale descriptor for shape representation, matching and retrieval. *Comput Vis Image Underst* 145:43–58
90. Yang C, Wei H, Yu Q (2016) Multiscale triangular centroid distance for shape-based plant leaf recognition. In: *ECAI*, pp 269–276
91. Yang C, Wei H, Yu Q (2018) A novel method for 2d nonrigid partial shape matching. *Neurocomputing* 275:1160–1176
92. Yang K, Chen Y, Zhang H, Liu X, Zhao W et al (2019) Robust point set registration method based on global structure and local constraints. *Digit Med* 5(2):76

93. Zhang D, Lu G (2005) Study and evaluation of different fourier methods for image retrieval. *Image Vis Comput* 23(1):33–49
94. Zhang D, Lu G et al (2002) A comparative study of fourier descriptors for shape representation and retrieval. In: *Proceedings of the 5th Asian conference on computer vision*, Citeseer, p 35
95. Zhang T, Li J, Jia W, Sun J, Yang H (2018) Fast and robust occluded face detection in atm surveillance. *Pattern Recogn Lett* 107:33–40
96. Zheng Y, Guo B, Li C, Yan Y (2019) A weighted fourier and wavelet-like shape descriptor based on idsc for object recognition. *Symmetry* 11(5):693
97. Zheng Y, Meng F, Liu J, Guo B, Song Y, Zhang X, Wang L (2020) Fourier transform to group feature on generated coarser contours for fast 2d shape matching. *IEEE Access* 8:90141–90152
98. Zuliani M, Bhagavathy S, Manjunath B, Kenney CS (2004) Affine-invariant curve matching. In: *2004 International conference on image processing, 2004. ICIP'04, vol 5, IEEE*, pp 3041–3044

**Publisher's note** Springer Nature remains neutral with regard to jurisdictional claims in published maps and institutional affiliations.

Springer Nature or its licensor (e.g. a society or other partner) holds exclusive rights to this article under a publishing agreement with the author(s) or other rightsholder(s); author self-archiving of the accepted manuscript version of this article is solely governed by the terms of such publishing agreement and applicable law.